2dFGRS and SDSS Galaxy Group Density Profiles

Eugenia Díaz[1,2], Ariel Zandivarez[2], Manuel E. Merchán[2] and Hernán Muriel[2]

Grupo de Investigaciones en Astronomía Teórica y Experimental, IATE, Observatorio Astronómico, Laprida 854, Córdoba, Argentina.

ABSTRACT

We have analysed the distribution of galaxies in groups identified in the largest redshift surveys at the present: the final release of the 2dF Galaxy Redshift Survey and the first release of the Sloan Digital Sky Survey. Our work comprises the study of the galaxy density profiles and the fraction of galaxies per spectral type as a function of the group-centric distance. We have calculated the projected galaxy density profiles of galaxy groups using composite samples in order to increase the statistical significance of the results. Special cares have been taken in order to avoid possible biases in the group identification and the construction of the projected galaxy density profile estimator. The results show that the projected galaxy density profiles obtained for both redshift surveys are in agreement with a projected Navarro, Frenk & White predictions in the range $0.15 < r/r_{200} < 1$, whereas a good fit for the measured profiles in the whole range of r/r_{200} is given by a projected King profile. We have adopted a generalized King profile to fit the measured projected density profiles per spectral type. In order to infer the 3-D galaxy density profiles, we deproject the 2-D density profiles using a deprojection method similar to the developed by Allen & Fabian. From 2-D and 3-D galaxy density profiles we have estimated the corresponding galaxy fractions per spectral type. The 2-D fraction of galaxies computed using the projected profiles show a similar segregation of galaxy spectral types as the obtained by Domínguez et al. for groups in the early data release of the 2dF Galaxy Redshift Survey. As expected, the trends obtained for the 3-D galaxy fractions show steeper slopes than the observed in the 2-D fractions.

Subject headings: galaxies: clusters: general — galaxies: statistics — methods: N-body simulations — methods: data analysis

---

[1]Agencia Nacional de Promoción Científica

[2]Consejo de Investigaciones Científicas y Técnicas de la República Argentina.

1. Introduction

Several models have been proposed to characterize the projected galaxy density in clusters of galaxies. Most of these models assume spherical symmetry and that the matter distribution is traced by galaxies. The first assumption can be true for a sub-sample of clusters, while the second is more difficult to quantify and is close related with different processes like galaxy formation, galaxy evolution, dynamical friction, etc. Assuming that the galaxy velocity dispersion is well represented by an isothermal sphere, King (1962) proposed a model to describe the galaxy projected density profile. More recently, Navarro, Frenk and White (1995, hereafter NFW95) analysing high-resolution N-body simulations propose an universal profile for dark matter halos. These authors found that their model can appropriately describe the mass density profiles for a large range of masses. The observational evidence coming from the giant arcs in clusters can be used to introduce constrains to the mass distribution in the core of clusters (Navarro, Frenk and White 1997). Strong lensing effects require a very small core radii, that in principle can be consistent with the NFW mass profile. Nevertheless, very high resolution cosmological simulations produce density profiles with inner slopes ~ -1.5 that are steeper than the obtained from NFW (slope of ~ -1 near the center) (Moore et al. 1998). It is not clear whether the galaxy density profile will follow the mass, in particular in the very core of clusters where the scales of galaxies impose the resolution limit. The controversy among different models to describe both, the mass and galaxy profile is still open and more observational evidences are needed.

Adami et al. (1998) studied the galaxy density profiles for an important sample of rich clusters of galaxies. One of the main clue of this work was to investigate whether the galaxy distributions have cores (like King profile) or cups (NFW profile). Based on redshift information taken from ENACS (ESO Nearby Abell Cluster Survey, Katgert et al. 1998) and projected galaxy distribution coming from COSMOS (MacGillivray & Yentis, 1994) Adami et al. 1998 conclude that in general the King profile provides a better representation of the data than the NFW profile.

Bartelman (1996) derived the analytic expression for the surface mass density of the NFW profile while Lokas & Mamon (2001) provide the tools for modeling the NFW profile and give predictions for different observational quantities. Independently of any analytical model the 3D profile can be derived applying a deprojection method similar to those implemented for the X-ray analysis of the hot intra-cluster gas (Allen & Fabian 1997).

Most of the previous analysis on galaxy density profiles consider galaxies regardless their properties. The effect of morphological segregation (MS), (Dressler 1980, Whitmore & Gilmore 1991, Dominguez, Muriel & Lambas 2001) implies that different galaxy populations will have different galaxy density profiles. MS works were carried out analysing the

bidimensional (2-D) galaxy fractions of different morphological types. In order to recover the 3D MS, the spatial (3-D) galaxy density profiles for each morphological type should be previously known. Salvador-Sole and Sanromà (1989) have analysed the observed correlation between morphological fractions and the projected density of galaxies. They found that this correlation is a consequence of an intrinsic 3D effect that is dependent on cluster concentration.

Using the Merchán & Zandivarez (2002) group catalog constructed from the early data release of the 2dF Galaxy Redshift Survey, Dominguez et al. (2002) derive the relative fraction of galaxies with different spectral types as a function of local galaxy density and group-centric distance. These authors found that for high mass groups ($M_V \gtrsim 10^{13.5} M_\odot$) a strong dependence of the relative fraction of spectral types on both, galaxy density and group-centric radius is observed.

The aim of this paper is to determine the projected and the 3-D galaxy group density profiles for different spectral types. We also derive the intrinsic 3-D MS that results from the observed 2-D MS. The observational results are compared with those obtained from different analytical models. This paper is outlined as follows: the deprojection method to apply on projected density profiles is described in section 2. The galaxy and group data in the 2dF Galaxy Redshift Survey and the Sloan Digital Sky Survey is quoted in section 3. The mock catalog tests made for the projected density profile estimator and the subsequent application to observational data are carried out in section 4. The derivation of the 3-D density profiles and the estimation of 3-D galaxy fractions are described in section 5. Finally, in section 6 we summarize our conclusions.

2. Density profiles in numerical simulations

2.1. Density profiles estimator

We use collisionless cosmological numerical simulations of flat, low density, cold dark matter universes performed using the Hydra N-body code developed by Couchman et al. (1995). Simulations are constructed with 128^3 particles in a cubic comoving volume of 180 h^{-1} Mpc per side starting at $z = 50$. The adopted cosmological model corresponds to an universe with a present day matter density $\Omega_m = 0.3$, vacuum energy density $\Omega_\Lambda = 0.7$, initial spectral slope $n = 1$, $\Gamma = 0.21$, Hubble constant $H_0 = 100\ h\ km\ s^{-1}\ Mpc^{-1}$ with $h = 0.7$ and an amplitude of mass fluctuations of $\sigma_8 = 0.9$.

Groups used in this section were, initially, identified using a standard friend of friend finder algorithm with density contrast of $\delta\rho/\bar{\rho} = 300$ corresponding to a linking length of

$d_0 = 0.15 \times n^{-1/3}$,where n is the mean density number of particles; after that we select high mass groups, spanning a mass range from 3.5×10^{13} to 5.8×10^{14} $M_\odot$ h^{-1}. The final sample consists of 690 groups.

In an attempt to increase the statistical significance, we combine all groups to produce a composite set of dark matter (DM) particles, properly scaled to take into account the different group sizes and masses. The composite sample was made assuming that all groups obey the same type of density profile but with different scales. Hence, it is necessary to introduce two parameters: one of them to normalize the group-centric distances and the other to normalize the masses. For convenience, we adopt the radius at which the mean interior density is 200 times the mean density of the universe (r_{200}) as the normalization scale and the mass contained in r_{200} (M_{200}) as the mass normalization.

We measure the projected density profile for the composite sample as a function of the normalized radii r/r_{200}. The binning scheme used through all this work is the equal number binning. The measured density profile will be compared with the analytical function obtained by NFW97. The 3-D NFW97 density profile is described by the following equation:

$$\frac{\rho(r)}{\rho_c} = \frac{\delta_c}{c\frac{r}{r_{200}}(c\frac{r}{r_{200}} + 1)^2} \tag{1}$$

where $\rho_c = 3H^2/8\pi G$ is the critical density for closure, c is the concentration of the halo, and δ_c is the characteristic density (see eq. 2 of NFW97). Through all this work we use a projection of the equation 1 obtained by numerical integration along the line of sight.

Upper panel of Figure 1 shows the projected density profile normalized to the number of groups involved in each bin (long dashed line) measured for the composite sample. The dot-dashed lines are the projected NFW profiles corresponding to different values of the c parameter (4.45 and 12.05). These c values are associated with a wide range of masses ($10^{11} < M/M_\odot < 10^{15}$). In the lower panel it can be seen, in long dashed line, the comparison between the measured profile and the analytical NFW profiles, plotted as the ratio Σ/Σ_{NFW}. Left to the vertical line in Figure 1 the densities are underestimated due to the uncertainty in the location of the group geometric center. An improvement of the group geometric center estimation can be obtained increasing $\delta\rho/\bar{\rho}$ in the group identification, which produces groups with geometric centers closer to the overdensity peaks. The measured projected density profile for groups identified with $\delta\rho/\bar{\rho} = 2000$ is plotted in the upper panel of Figure 1 (short-dashed line). This profile has a very good agreement with the NFW predictions. We also show in dots the density profiles for each group. This procedure for improving the group geometric center is not feasible in observational surveys, since the number of groups identified is strongly decreased for high overdensities and this affects the reliability of the

results. Hence, it is important to find another method to correct the group center positions and keeping constant the number of groups. The procedure adopted for the estimation of the new group centers takes into account the projected local number densities at the position of each particle (galaxy, when dealing with observational data). A first estimation of the center is obtained by the following equation:

$$r_c^{(1)} = \frac{\sum_{j=1}^{N} \rho_j^{PL} r_j}{N \bar{\rho}^{PL}} \tag{2}$$

where N is the number of particle members of each group, ρ_j^{PL} is the projected local density in the position of the j^{th} particle and $\bar{\rho}^{PL}$ is the mean projected local density. The projected local density for the j^{th} particle is computed using the projected circular area which contains the n nearest particles. We use the values of $n = 75$ in the simulation and $n = 5$ in the catalogs (Domínguez et al. 2002). This procedure improves the center location, but in some cases it is not enough to match the identified group centers with the corresponding overdensity peaks. Consequently, we adopt an iterative procedure as follow:

1. Using the geometric center position (r_b) we determine the distance d_0 to the farthest particle/galaxy.

2. After the computation of $r_c^{(1)}$ we reject all the particles/galaxies with distances to $r_c^{(1)}$ greater than d_0. Then we estimate d_1 for the remaining particles/galaxies.

3. We calculate $r_c^{(2)}$ for the new group using the equation 2 and applying the same procedures as described in item 2.

The iteration must go on until $d_{M-1} = d_M$. Finally, after M iterations, the group center obtained is $r_c = r_c^{(M)}$. Besides the improvement in the determination of the center position, the proposed method also correct the group merging problem produced by the process of identification, in other words, groups with two or more overdensity peaks are cleaned, preserving the highest peak.

We use this method to determine the centers for the groups identified with $\delta\rho/\bar{\rho} = 300$. The density profile obtained for the corrected sample is shown in solid line in the upper panel of Figure 1. It can be seen that our center estimator allows us to reproduce the density profile obtained using $\delta\rho/\bar{\rho} = 2000$, with the advantage of keeping constant the number of groups identified with $\delta\rho/\bar{\rho} = 300$. The agreement with the NFW predictions can also be observed in the lower panel of this Figure (solid line curves).

2.2. Deprojection method of density profiles

From the projected density profile we calculate the 3-dimensional profile applying a deprojection method similar to that developed by Allen & Fabian (1997). The deprojection analysis assumes spherical symmetry. The method is a matter of dividing the spatial distribution into a series of n concentric spherical shells. The projected number of galaxies $N(j)$ in the jth cylindrical bin can be considered as the contribution of different spherical shells, which can be calculated as the 3-D numerical density of each shell, $\eta(j)$, multiplied by the corresponding volume $V_{j,i}$:

$$N(j) = \sum_{i=j}^{n} \eta(i) V_{j,i} \quad ; \; 1 < j < n \; , \quad j < i < n \tag{3}$$

where $V_{j,i}$ is the volume corresponding to the intersection of a spherical shell with inner radius r_{i-1} and outer radius r_i and a cylindrical shell with radii r_{j-1} (inner) , r_j (outer). Since the projected density in the last cylindrical shell is only dependent on the 3-D density of the outer spherical shell, equation 3 can be used to obtain the 3-D density profile $\eta(j)$ from outer to inner shells:

$$\eta(j) = (N(j) - \sum_{i=j+1}^{n} \eta(i) V_{j,i}) / V_{j,j} \tag{4}$$

In order to test the method reliability we apply it to the composite sample made with DM groups identified in N-body simulations. The derived 3-D density profile is shown in Figure 2 (solid line) and it is compared with the 3-D profile directly measured in simulations. From this comparison we can observe a perfect recover of the 3-D density profile.

3. The data

3.1. The galaxy sample

At present, the largest samples of galaxies with spectroscopic redshift determinations are the 2dFGRS (2 degree Field Galaxy Redshift Survey) and the SDSS (Sloan Digital Sky Survey). In this work we use both catalogs in order to obtain the largest samples of groups and increase the reliability of our results.

The 2dF survey covers 1500 deg^2 with a median depth of $\bar{z} = 0.11$. The complete 2dFGRS consists of 221414 galaxies in two declination strips and 2-degree random fields scattered around the southern galactic pole (SGP) strip. The galaxies were taken from an

improved version of the APM galaxy survey (Maddox et al., 1990a,b; Maddox, Efstathiou & Sutherland, 1996). The sky coverage of the 2dFGRS is not uniform (a detailed completeness description is given by Colless et al., 2001; see also http://www.mso.anu.edu. au/2dFGRS/). Galaxies in this survey also have a spectral classification given by the parameter η based on a principal component analysis as described by Madgwick et al. (2002).

Recently, the Sloan Digital Sky Survey has validated and made publicly available the First Data Release (Abazajian et al. 2003) which is a photometric and spectroscopic survey constructed with a dedicated 2.5 m telescope at Apache Point Observatory in New Mexico. The First Data Release consist of 2099 deg^2 of five-band (u g r i z) imaging data and 186240 spectra of galaxies, quasars and stars. In this work we mainly use the spectroscopic sample. The SDSS Team has found that the survey redshift accuracy is better than 30 $km\ s^{-1}$. Our sample comprises 100118 galaxies with radial velocities spanning the range 420 $km\ s^{-1} \leq V \leq 90000\ km\ s^{-1}$ and an upper apparent magnitude limit of 17.77 in the r-band. In order to work with different kinds of galaxy population, we compute a galaxy spectral type based on a Principal Component Analysis (PCA), using a cross-correlation with eigentemplates constructed from SDSS spectroscopic data. These spectral types are computed with the first two eigencoefficients as recommended by de SDSS Team.

3.2. The group samples

The group samples obtained from the 2dFGRS and SDSS were constructed using an algorithm similar to that developed by Huchra & Geller (1982). Particularly, we have introduced some modifications in the group finder in order to take into account the sky coverage of the 2dFGRS. The adopted procedure is the same as described by Merchán & Zandivarez (2002) who consider the redshift completeness, magnitude limit and μ masks of the 2dFGRS. The identifications were carried out using a density contrast of $(\delta\rho/\bar{\rho})_z = 80$ and a line of sight linking length of $V_0 = 200 km\ s^{-1}$.

As was detailed in section 2, the group center location has an important influence on the density profiles estimations. It is known that working on observational redshift surveys means that group identification must be performed in redshift space. This sort of procedure could induce missidentifications of groups respecting to those that would be identified in real space. For instance, the group finder algorithm in redshift space can not completely eliminate the interloper effect on the identification. This effect is likely to produce an artificial increment in the projected size of groups or the detection of fictitious systems with multiple overdensities. In order to understand the relation between groups identified in real and redshift space we perform a comparative study using mock catalogs (see section 4 for a detailed description

of mock catalogs construction). The groups identification in real space was performed using a similar algorithm as the adopted for redshift space, but using the same linking length in both, transverse and radial directions. Right upper panel in Figure 3 shows a comparison among the groups identified in both, real space (open circles) and redshift space (crosses) using $\delta\rho/\bar{\rho} = 80$, for a given patch in the sky. Points represent the galaxies/particles in this region identified as group members in redshift space. As can be seen, several groups in real space were joined in a single group in redshift space. Our purpose is to reproduce the groups identified in real space with $(\delta\rho/\bar{\rho})_r = 80$. In order to do this, we have carried out a second identification on the previous group sample identified in redshift space, varying the density contrast, $(\delta\rho/\bar{\rho})_z$, until we observe a similar identification as the obtained in real space. Lower panel in Figure 3 shows the same comparison as the one plotted in the right upper panel, but here crosses are the groups obtained after a second identification in redshift space with a density contrast of $(\delta\rho/\bar{\rho})_z \sim 315$. Even though the second identification does not perfectly reproduce the one obtained in real space, our study indicates that the $(\delta\rho/\bar{\rho})_z$ adopted for the second identification is the best choice to produce a sample of groups quite similar to the observed in real space. Consequently, we have performed a second identification, using the best density contrast value previously obtained, over the group samples of the 2dFGRS and SDSS described before. Finally, the group centers were computed using the iterative method detailed in section 2. The group samples used through this work include systems with masses greater than $6 \times 10^{13} h^{-1} M_{\odot}$ and having more than 10 galaxy members. The adopted mass threshold, only selects the more massive groups that are the most interesting when spectral type properties are studied (Domínguez et al., 2002). The final samples comprise 132 groups for the 2dF and 86 for the SDSS. The group physical properties were computed using the same formulas adopted by Merchán & Zandivarez (2002). The median group properties and the widths of the distributions (semi-interquartile range) are quoted in Table 1. Analysing the information shown in this table it can be seen that the average properties are very similar for both catalogs. This is an expected result taking into account the similarities of both catalogs.

4. Projected galaxy density profiles

In order to measure projected galaxy density profiles we use a similar procedure to that employed in the simulations taking into account the surveys limitations. We construct the composite samples for both group catalogs adopting r_{200} as the normalization scale and M_{200} as masses normalization. The computation of r_{200} was made following Carlberg et al.(1997):

$$r_{200} = \frac{\sqrt{3}}{10} \frac{\sigma}{H(z)} \tag{5}$$

while M_{200} was obtained using (see appendix of NFW97):

$$M_{200} = \left(\frac{r_{200}}{K} \left(\frac{\Omega_0}{\Omega(z)} \right)^3 (1+z) \right)^3 \; h^{-1} \; M_\odot \tag{6}$$

where $K = 1.63 \times 10^{-5} h^{-1} Mpc$. These scaling relations are in very good agreement with the properties directly measured from the individual DM groups.

Working with observational samples require to have particular considerations when constructing density profiles, specially when seeking for the largest statistical sample. As was noticed by Whitmore, Gilmore & Jones (1993, hereafter WGJ93), a magnitude cutoff decreases the number of galaxies while affects the mix of spectral types since the luminosity functions are different for each type. Distant systems will only include the brightest galaxies , which tend to be the earlier, resulting in an incomplete source of information. A magnitude cutoff correction is made following WGJ93 where a weight is given to each galaxy. This weight is a function of the redshift, the spectral type and the catalog apparent magnitude limit, and it is given by the following equation:

$$w(z, m_l) = \left[\frac{\int_{-\infty}^{M_l(z)} \Phi(M) dM}{\int_{-\infty}^{M_l(z_c)} \Phi(M) dM} \right]^{-1} \tag{7}$$

where $\Phi(M)$ is the luminosity function per spectral type of galaxies in groups, $M_l(z) = m_l - 25 - 5log(d_L) - (k+e) + 5log(h)$ the absolute magnitude, d_L is the luminosity distance, m_l the catalog apparent magnitude limit and z_c is chosen as a typical redshift for groups in the sample.

4.1. Mock catalogs

4.1.1. Angular Masks

Since the sky coverage of the 2dF group sample is not uniform, we need to make extra-corrections before measuring the projected density profiles. With the aim of determining and testing the corresponding corrections to the observed sample, we use four types of mock catalogs. Each of these mocks corresponds to different sky coverage as in Merchán & Zandivarez (2002). So, we study the influence on the density profiles of each distinctive feature present in the catalog. To increase the statistical strength we construct a set of ten mock catalogs for each type from ten cosmological simulations with different initial conditions (section 2). Given the periodicity of the simulation box we locate the observer at an arbitrary position and repeat the box until the survey extent is completed. These

catalogs are constructed using a bias scheme $b = 1$ between DM particles and galaxies which is quite accurate to reproduce the clustering of the data mainly on large scales. Adopting the galaxy luminosity function given by Norberg et al. (2002) we assign absolute magnitudes to particles obtaining mock catalogs with the same selection function than the observed for the 2dFGRS.

The first set of mock catalogs (mock-m) introduces a fixed faint survey magnitude limit, $m_l = 19.2$. We identify groups in this mock in the same way as in the 2dF sample (groups with masses greater than $6\times10^{13}M_{\odot}$, and having more than 10 members). After constructing the composite sample (as explained in section 2) we measure the projected density profile counting galaxies weighted by the equation 7. The projected density profiles measured for each mock catalog were averaged and the corresponding mean profile is shown in the left upper panel in Figure 4 (points). This profile is compared with the projected density profile computed from the DM groups identified in the N-body simulations (solid line).

The second set of mock catalogs (mock-m-c) has also a fixed faint survey magnitude limit but adding the effect of redshift completeness as in the real survey. The procedure to make the composite sample of groups is the same in all cases. At this time, we put another weight to the galaxies in order to measure the projected density profile. This weight is the result of multiplying $w(z, m_l)$ by the redshift completeness $c(\alpha, \delta)$ available from the 2dF mask. In Figure 4, right upper panel shows the averaged profile corresponding to this set of mock catalogs (mock-m-c).

The third set of mock catalogs (mock-m_v) has a faint survey magnitude limit depending on the angular position of a particle consistent with the apparent magnitude limit derived from the 2dF mask. To measure the projected density profile we introduce a weight $w(z, m_v)$ that take into account the variable magnitude limit in the calculation of $M_l(z)$. The averaged density profile is shown in Figure 4 (left lower panel).

Finally we use a last set of mock catalogs (mock-c-m_v) which has both effects, the variable magnitude limit and the redshift completeness masks. In this case, the weight assigned to each galaxy consists in the multiplication by both weights, $w(z, m_v)$ and $c(\alpha, \delta)$. The mean profile is shown in the right lower panel in Figure 4. Error bars in Figure 4 are computed measuring the 1-σ dispersion over each set of ten mock catalogs used to obtain the average density profiles. The inset panels show the ratio between the averaged projected density profiles for each set of mock catalogs and the projected density profile measured for the DM groups identified in the N-body simulation. From these panels we observe that we are able to recover the profiles obtained for the simulation making the appropriated corrections on each mock catalog.

4.1.2. Missing Pairs

In the observational process of the SDSS sample, there is a restriction in the targeted objects since the fiber centers can not be placed closer than 55″ on a given plate. This limitation produces the missing-pair problem, so that, one of the pair components can not be observed. The loss of galaxies was quantified by Strauss et al. (2002), showing that about the 6% of the galaxies are not observed owing to the missing-pair problem. This percentage represents roughly the 70% of the total number of galaxy pairs, while the remaining 30% was measured due to the overlapping of plates in some regions. In order to analyze the possible effect of this loss of galaxies on the resulting projected density profile we work with mock catalogs. We construct two SDSS mock catalogs from N-body simulations (section 2.1) following a similar prescription as the adopted for the 2dF mocks, but using the luminosity function computed by Blanton et al. (2003). In one of these catalogs (mock-sp) we reproduce the missing-pair problem of the SDSS sample. This was achieved selecting the 70% of the galaxy pairs and subsequently we remove one component of each pair in this subsample. We measure the projected density profiles for both mock catalogs following the procedure used for the mock-m of the previous section. Figure 5 shows the comparison among these density profiles. Circles are the projected density profile measured in the SDSS mock catalog with the full sample of pairs, while the squares correspond to the profile obtained from the mock catalog affected by the missing-pair problem. This figure shows that this problem produces a significant variation on the projected density profile mainly in the inner regions of groups, biasing the sample towards profiles with a core. We develop a method to correct this effect adding random galaxies to the sample of group galaxies. The outline of the method is as follows:

1. We seek for the 30% of existing pairs in the galaxy catalog for which both members were observed: N_1 (number of galaxies in pairs with distances less than $D^*_{m_{SDSS}} = 55''$).
2. We identify which of the N_1 galaxies belong to groups: N_2
3. We calculate the percentage of galaxies in pairs that are group members: $P_1 = N_2/N_1$. Here we have assumed that the probability of measuring both members of a galaxy pair does not depend on whether it is in a group or not.
4. Using that N_1 is the 30% of the full sample of pairs, we estimate the number of galaxies in pairs that belongs to the remaining 70%: $N_3 = 7/3 \times N_1$
5. We calculate how many of the N_3 galaxies would be found in groups: $N_4 = N_3 \times P_1$
6. Finally, the number of galaxies to introduce in the sample is $N_5 = N_4/2$ since we already have one of the pair component in the sample.

7. Using the galaxies in pairs that belongs to groups (N_2), we measure its redshifts and r/r_{200} distributions relative to the center of the group to which each of the galaxies belong.

8. For the computation of the projected density profiles, we randomly add N_5 galaxies reproducing the previous distributions.

We apply this procedure to the mock-sp, and measure the corresponding density profile, which is also shown in Figure 5 (triangles). It can be observed that our method is capable to correct the missing-pair effect on density profiles. We will use this method in the SDSS group sample in the following sections in order to obtain a fair estimate of the projected density profiles.

For correcting the missing-pair problem in the 2dF sample we apply the 8-step procedure described above where the values used for the SDSS must be changed: in items 1 and 4 $(30\%)_{SDSS} \rightarrow (85\%)_{2dF}$; item 4 $(70\%)_{SDSS} \rightarrow (15\%)_{2dF}$ and in item 1 $(55'')_{SDSS} \rightarrow (50'')_{2dF}$. The rest of this subsection describes how we find the percentage of lost galaxies in pairs (15%) and the maximum distance to define the missing-pair problem (50″) for the 2dF sample. We first measure two distance distributions: the first is the distribution of distances from each galaxy to its closest neighbor (D_m) among galaxies that belong to the input catalog of the 2dFGRS (Colless et al., 2003); the second distribution was built from a subsample of the previous one. This subsample (2dFI-2dF) comprises all the galaxy pairs in the input catalog that were not completely surveyed by the 2dFGRS. Their cumulative distributions are shown in the upper panel of Figure 6. The solid line corresponds to the input catalog while the dotted line is the histogram for the subsample 2dFI-2dF. The ratio among these cumulative distributions is the fraction of lost galaxies in the 2dF until a given angular distance. This loss is due to two issues in the observational process: the sky coverage of the sample and the missing-pair problem. There is a scale beyond which the ratio of missed pairs has to be constant as function of D_m, as there is for both input catalog and redshift catalog a maximal D_m value. Indeed, by definition D_m is the minimal distance to a neighbor, which has to reach a maximal value in a finite sample. Therefore beyond D_m^{max} the ratio is constant. That constant value correspond to the incompleteness due to the sky coverage and it has to be subtracted from the ratio in order to obtain an estimate of the close pair incompleteness.

The resulting fraction as a function of D_m is shown in the lower panel of Figure 6. From this plot we should be able to determine the fraction of lost galaxies but, firstly, it is necessary to know the angular distance $D^*_{m_{2dF}}$ so it is representative of the largest number of the galaxies that were missed due to the missing-pair problem. In order to determine $D^*_{m_{2dF}}$ we calculate the number of galaxies that must be added until a given angular distance D_m. These numbers are calculated for each D_m following the steps 1 to 6, previously described for the correction

of the missing-pair problem. The fraction of lost galaxies involved in this procedure are obtained from the lower panel of Figure 6. Then, the resulting numbers of galaxies that must be added until a given angular distance D_m are shown in the inset panel of the lower panel of Figure 6. From this distribution we determine $D^*_{m_{2dF}} = 50''$ that corresponds to the D_m where the distribution is maximum. This is the optimal way to determine the $D^*_{m_{2dF}}$ since this value allows us to compute the appropriate correction to the projected density profiles. This was tested constructing a mock catalog with a similar sky coverage to that observed in the 2dFGRS and an enhanced pair incompleteness. The later characteristic is necessary to obtain a large enough effect so it can be measured in the projected density profile. As in the case of the SDSS, we observe that the missing-pair underestimates the amplitude of the density profile in the inner region. After performing a similar analysis to that shown in Figure 6 but using the mock catalog, we observe that introducing the maximum number of galaxies (ie., the peak of the distribution in the lower inset panel) allow us to recover the true density profile. This result confirms that the procedure adopted to obtain the value of $D^*_{m_{2dF}}$ is the optimal. To conclude, we observe that using $D^*_{m_{2dF}} = 50''$ means that the 2dFGRS losses approximately 15% of the galaxies (it implies that 2dF has lost $N_5 = 87$ pair-members from the sample of galaxies in groups used in this work).

The missing-pair correction is an important issue to be considered when working on the SDSS (it looses the 70% of the galaxy pairs). The density profiles with and without this correction are different mainly in the inner regions. On the other hand, the correction applied to the 2dFGRS (15% of the galaxy pairs) will not introduce a significant change in the resulting density profile (see Fig. 8 and references in the next section).

4.2. 2dF and SDSS projected density profile

Once we have corrected the samples by the missing-pair problem, we construct the composite samples and split galaxies in 3 spectral types. For the 2dF sample we use the classification made by Madgwick et al.(2002) to spectral types. This classification is determined by the shape of the η-distribution:

- Type 1: $\eta < -1.4$,
- Type 2: $-1.4 \leq \eta < \ 1.1$,
- Type 3+4: $\eta \geq \ 1.1$.

The first type is dominated by elliptical and early-type spiral galaxies, getting later toward type 3+4.

In an attempt to obtain a similar spectral type classification for the SDSS group sample, we seek for a correlation between the spectral parameters η of the 2dF and τ of the SDSS comparing 3300 galaxies that both have in common. We find a roughly linear behavior among both parameters (Figure 7). The fit obtained for this relation is:

$$\tau = (0.065 \pm 0.002) \times \eta + (0.056 \pm 0.003) \tag{8}$$

Using this relation we divide the SDSS sample into 3 spectral types according to the classification made for the 2dF. Hence the resulting classification for the SDSS sample is:

- Type 1: $\tau < -0.035$,
- Type 2: $-0.035 \leq \tau < 0.128$,
- Type 3+4: $\tau \geq 0.128$.

We measure the projected density profiles for the composite samples (the whole sample and the samples selected per spectral type). The procedures to introduce weights in the estimation are the same as the used in mock-c-m_v for the 2dF and using the equation 7 for the SDSS. For the 2dF sample we adopt the luminosity functions per spectral type of galaxies in groups given by Martínez et al. (2002) and $k + e$ corrections given by Norberg et al. (2002). For the SDSS we use the luminosity functions per spectral type of galaxies in groups estimated following the same procedure as described by Martínez et al. (2002). The $k + e$ corrections as a function of redshift were estimated following a method similar to that described by Norberg et al. (2002), using the code of stellar population synthesis developed by Bruzual & Charlot (1993).

Figures 8 and 9 show projected density profiles for the 2dF and the SDSS composite samples, respectively. The left upper panels show the profiles for the whole sample (points). The open circles are the projected density profile measured without correcting by the missing-pair problem. As we mentioned in the previous section, the effect is not significant for this sample. Error bars in these panels were calculated computing the mean dispersion obtained using sets of 10 mock catalogs. The remaining three panels correspond to projected density profiles per spectral types (points) where error bars are computed performing a bootstrap resampling of the data.

In the left upper panels of both Figures we confront the measured projected density profiles for the complete samples against two analytical NFW projected density profiles (dot-dashed lines). Any profile corresponding to groups with masses between $10^{11} M_{\odot}$ and $10^{15} M_{\odot}$ should lie in the region determined by these two NFW profiles. From the comparison,

we can notice that the dark matter NFW profile does not show the same behavior as the obtained from galaxy samples in the inner regions of the galaxy groups. We also compare our results with the analytical prediction for galaxy density profiles given by King (1962). We fit the data points using a generalized King profile given by the formula:

$$\Sigma_m(r) \propto \frac{1}{(1+(c(\frac{r}{r_{200}}-x_0))^2)^\beta} \tag{9}$$

where c is the concentration parameter defined as r_{200}/r_{core}, β is the slope in the outer region and x_0 is the radius where the profile reaches its maximum value. These parameters are determined using the Levenberg-Marquardt method (Press et al., 1986). This method takes into account data errors and applies a minimum non-linear least squares procedure. The number of parameters to fit is chosen to be as low as possible. Notice that the King (1962) projected profile is obtained by setting $\beta = 1$ and $x_0 = 0$. Using a mean value of r_{200}, and a range for r_{core} from 100 to 300 $kpc\ h^{-1}$ then the allowed values of c parameter are in the range $4 - 13$. The best-fitting parameters obtained for the full sample and for each spectral type are listed in Table 2. These fits are shown with solid lines in Figures 8 and 9. The dotted lines show the King-fit obtained for the whole sample.

In order to quantify the goodness of the fits we compute the probability Q which is a function of the χ^2 and the degree of freedom of the distribution ν (Press et al., 1986). The chi-square probability $Q(\chi^2, \nu)$ is an incomplete gamma function and gives the probability that the chi-square should exceed a particular value χ^2 by chance. For a fit with M free parameters ($\mathbf{a}$) the χ^2 is calculated using

$$\chi^2 = \sum_{i=1}^{N_{bin}} \left(\frac{\Sigma_i - \Sigma_m(\frac{r}{r_{200}}; \mathbf{a})}{\sigma_i} \right)^2 ; \quad \mathbf{a} = (a_1, a_2, ..., a_M) \tag{10}$$

while the number of degrees of freedom of the distribution is computed as $\nu = N_{bin} - M$. Using the $Q(\chi^2, \nu)$ value, the goodness of a fit is quantified in the following way: a value of $Q > 0.1$ says that the fit is a very good reproduction of the data distribution; if the value is in the range $0.001 < Q < 0.1$ then the fit is acceptable and finally, if $Q < 0.001$ the model poorly fit the data. It should be remarked that this kind of test is also valid even when the models are not strictly linear in the $a's$ coefficients. In the last column of Table 2 we quoted the Q values of all fits in both samples. From these values we conclude that almost all the fits obtained are a very good approximation to the measured projected density profiles and only one of them is in the range of acceptable. As an important result we can observe, in left upper panel of Figures 8 and 9, that the King profile is a good descriptor of the observational data in the whole range of r/r_{200} and the c values are within the allowed range. This result is consistent with the obtained by Adami et al. (1998) who found that the King profile provides a better fit to the galaxy density profile than the NFW profile. This

result can be more clearly observed in the inset box in the upper left panel of these figures. In these panels we show the ratio between the observational projected density profile and the King profile (solid line). In dotted lines are also shown the ratio between the observational density profile and the NFW predictions. These figures show that NFW predictions differ from unity in the inner regions whereas King fits are roughly constant in the whole range.

Based on the projected density profiles for each spectral type, we calculate the relative fraction of galaxies with different spectral types as a function of the projected group-centric distance. This fraction is computed as the ratio between the projected density profile for a particular spectral type and the total projected density profile. In order to measure these ratios, we have rebinned the data, using a linear interpolation. Figure 10 shows the galaxy fractions for the 2dF composite sample (upper panel) and for the SDSS composite sample (lower panel). Using error propagation method, the error in the relative fraction of the type j for each bin is defined by the following equation:

$$\sigma_{frac_j} = \sqrt{(\sigma_{\Sigma_j}/\Sigma_T)^2 + (\sigma_T \Sigma_j/\Sigma_T^2)^2} \tag{11}$$

where Σ represents the projected density profile, and σ_Σ represents the error in these profiles. Thick lines in these Figures correspond to galaxy fractions calculated using the fits (Table 2) obtained for the projected density profiles per spectral type. The results are similar to that found by other authors when considering spectral types (Domínguez et al. 2002) or morphological classifications (Whitmore & Gilmore 1991, WGJ93). We observe in both, the 2dF and the SDSS group sample, that for small r/r_{200} radii the fraction of early type galaxies (Type 1) rises rapidly whilst the fraction of late type galaxies tends to be more important in the outerskirt of the galaxy systems. By comparing these panels we observe that the behavior of each type for both samples is quite similar and the main difference is only in the amplitudes. This difference is expectable because the samples are selected in different band magnitudes: $r-$band for the SDSS and b_j-band for the 2dFGRS. Therefore the percentage of low star forming galaxies (type 1) is going to be higher in the SDSS than in the 2dF whilst the opposite is found for the star forming galaxies (type 3+4).

5. 3-D galaxy fractions

One of the aims of this work is to derive information about the 3-D galaxy distributions from observational data. To achieve this aim we use the deprojection method described in section 2 to obtain the 3-D galaxy density profiles from the projected ones. The deprojection method produces very good estimates when we are dealing with projected profiles without bin to bin fluctuations, as it was the case in section 2 for N-body simulations. Nevertheless,

if the profiles show bin to bin fluctuations, this method tends to enhance the noise in the resulting profiles, from outer to inner radii of galaxy systems. For instance, Figure 11 shows the averaged deprojected density profiles corresponding to the deprojection of the 2-D profiles of ten mock catalogs of each kind (the averages of these 2-D profiles are shown in Figure 4). It can be seen that 3-D profiles present an important dispersion. Therefore, it must be expected that the intrinsic noise observed for the projected density profiles in the 2dF and SDSS catalogs will be amplified by the deprojection method. We carry out the deprojection of all the observed 2-D profiles measured in the previous section, obtaining noisy 3-D profiles. In order to estimate errors to these profiles, we perform bootstrap resampling of the 2-D data and then we deproject each bootstrap density profile. By calculating the 1-σ dispersion of the 3-D bootstrap profiles, the errors for the 3-D profile of the data are obtained. From the deprojected profiles we calculate the 3-D galaxy fraction per spectral type. These fractions can be seen in Figure 12 for the 2dF (upper panel) and SDSS (lower panel) samples, where the error bars are calculated by error propagation as in the 2-D case (equation 11). We decide to join the types 2 and (3+4) because the resulting noise of the deprojection does not allow to observe differences among them. It should be noticed that the importance of this result resides in the fact that these 3-D fractions are obtained by directly inverting the 2-D profiles, it means, without assuming a particular shape for the density profile.

Finally, we also show in Figure 12 the 3-D fractions per spectral type calculated analytically (thick lines). The analytical profiles that are needed for the computation of these fractions come from integrating the analytical fits of the 2-D density profiles assuming spherical symmetry. The result of the integration shows that the 3-D profiles keep the same functional form that the adopted for the 2-D case (generalized King), with values of $c_{3D} = c_{2D}$ and $\beta_{3D} = \beta_{2D}+0.5$. In this Figure it can be observed that the analytical curves present the same behavior that those obtained from the direct deprojection, indicating that the generalized King density profiles are also a good fit for the observational result in the 3-D case.

6. Summary and Conclusions

Using the two largest galaxy redshift surveys presently available, the final release of the 2dFGRS and the first release of the SDSS, we carry out an analysis of the galaxy populations and their distribution in massive groups of galaxies. Group identification on these surveys is made using an algorithm similar to that developed by Huchra & Geller (1982). Particularly, for the 2dFGRS sample, we introduce modifications, in order to take into account the non-uniform sky coverage of this survey (Merchán & Zandivarez, 2002). From a careful study of groups identified in mock catalogs we realized that this method

could produce false identifications in redshift space, producing an artificial enhancement of the group sizes or merging small systems in larges artificial groups. To solve these problems we identify groups upon the previous group sample, varying the density contrast until the redshift space identification is capable to reproduce the identification obtained in real space using $\delta\rho/\bar{\rho} = 80$. The new density contrast found in mock catalogs is used to perform a second identification in the 2dF and SDSS group samples. The group centers are estimated using an iterative method, which is capable to locate the group centers upon the overdensity peaks. We also correct the group samples for the missing-pair problem.

Once we have reliable group samples, we proceed with the analysis of the galaxy distribution in galaxy groups. This analysis comprise the study of density profiles for high mass groups. These profiles are derived using composite samples which are a combination of all groups in each catalogs. The normalization scale used to conform the composite sample is r_{200}, the radius at which the interior density is 200 times the mean density of the universe, and the mass normalization is M_{200}. The results found in this work do not depend on the normalization scale. Since the group samples used in this work are magnitude limited, our estimator of the projected galaxy density profiles is developed introducing weights in the galaxy counts which take into account a fixed or variable apparent magnitude limit and variations in the redshift completeness. The way of introducing these corrections was tested in mock catalogs, obtaining a good agreement with the density profiles derived from DM groups identified in the N-body simulations. The galaxy projected density profiles obtained for the 2dF and SDSS show a similar behavior. From the comparison of our results with the analytical projected NFW, we observe that the last fails to describe the behavior of the observational results in the inner region of groups. This seems to indicate that the dark matter profile (NFW) is not appropriated to describe the density profile traced by the luminous matter in the very core of galaxy groups. We observe that the King profile is a better fit for the observational data in the whole range of group-centric distances where the profiles can be measured, in agreement with the results of Adami et al. (1998). This result is also found when the normalization scale is modified, for instance, using any intrinsic projected group size as a normalization scale. We tested this point using the virial radii and the rms projected physical separation of galaxies from the group center. The use of these new normalization scales (r_{new}) produces the same β_{new} parameters that we obtain using r_{200} as a normalization scale. The c_{new} parameters are just a re-scaling of the previous and they are given by: $c_{new} = c_{200} \times \frac{r_{new}}{r_{200}}$.

We obtain that the resulting density profiles are reliable for $r/r_{200} > 0.03$, it was calculated taking into account the minimum distance between pairs of galaxies or the mean galaxy size, both at the mean distance of the galaxy systems. This constrain does not change our results since the fits are made from $r/r_{200} = 0.03$ to higher values. Then, we can claim that

the presence of a core in the projected density profiles is an intrinsic property of these galaxy systems and not a result of a biased measurement.

We also measure the projected density profiles per spectral type in both samples. In order to obtain analytical functions to describe the observational results, we adopt a generalized King profile to fit them. These results could be used as a tool to constrain semi-analytical models. The general galaxy density profile and the dependence of the density profiles on the spectral types must be correctly reproduced by the models.

Based on the available spectral type information, we compute the galaxy fractions per spectral type as a function of the normalized group-centric distance r/r_{200}. Our results are in good agreement with the previously obtained by other authors (Whitmore & Gilmore, 1991, WGJ93, Domínguez et al., 2002): the fraction of early type galaxies decreases when r/r_{200} increases whereas the opposite behavior is observed for the fraction of later types.

Using the obtained 2-D density profiles, we calculate the 3-D galaxy density profiles from their projected counterpart using a deprojection method similar to the one developed by Allen & Fabian (1997). The 3-D galaxy fractions are computed from the deprojected density profiles per spectral type. By comparing the 2-D and 3-D galaxy fractions it can be seen that the MS effect is more pronounced when 3-D fractions are analysed. Finally, the analytical 3-D fractions are calculated from the fits obtained for the 2-D density profiles. It is found a good agreement with the 3-D fractions directly calculated without assuming an analytical 2-D density profile.

Special thanks to the anonymous referee, for helping us to improve the original version of this work. We thanks to Julián Martínez for help us in the calculation of the $k + e$ correction for the SDSS and Cinthia Ragone for reading the manuscript. We also thank to Peder Norberg and Shaun Cole for kindly providing the software describing the mask of the 2dFGRS and to the 2dFGRS and SDSS Team for having made available the actual data sets of the sample. This work has been partially supported by Consejo de Investigaciones Científicas y Técnicas de la República Argentina (CONICET), the Agencia Nacional de Promoción Científica, the Secretaría de Ciencia y Técnica de la Universidad Nacional de Córdoba (SeCyT), the Agencia Córdoba Ciencia and Fundación Antorchas, Argentina.

REFERENCES

Abazajian , et al, 2003, AJ, 126, 2081

Adami, C., Mazure, A., Katgert, P., Biviano, A. 1998, A&A, 336, 63

Allen, S. W., Fabian, A. C. 1997, MNRAS, 286, 583

Bartelmann, M. 1996, A&A, 313, 697

Blanton, M. R., et al. 2003, ApJ, 592, 819

Bruzual, A. G., Charlot, S. 1993, ApJ, 405, 538

Carlberg, R. G., et al. 1997, ApJ, 478, 462

Couchman, H. M. P., Thomas, P. A., Pearce, F. R. 1995, ApJ, 452, 797

Dressler, A. 1980, ApJ, 236, 351

Domínguez, M., Muriel, H., Lambas, D. G. 2001, AJ, 121, 1266

Domínguez, M., Zandivarez, A., Martínez, H. J., Merchán, M. E., Muriel, H., Lambas, D. G. 2002, MNRAS, 335, 825

Huchra, J. P., Geller, M. J. 1982, ApJ, 257, 423

Katgert, P., Mazure, A., den Hartog, R., Adami, C., Biviano, A., Perea, J. 1998, A&AS, 129, 399

King, I. 1962, ApJ, 67, 471

Lokas, E., Mamon, G. 2001, MNRAS, 321, 155

MacGillivray, H. T., Yentis, D. J. 1994, IAUS, 161, 632

Maddox, S. J., Efstathiou, G., Sutherland, W. J., Loveday, J. 1990a, MNRAS, 242, 43P

Maddox, S. J., Efstathiou, G., Sutherland, W. J., Loveday, J. 1990b, MNRAS, 243, 692

Maddox, S. J., Efstathiou, G., Sutherland, W. J. 1996, MNRAS, 283, 1227

Madgwick, D. S., et al (2dFGRS Team), 2002, MNRAS, 333, 133

Martínez, H. J., Zandivarez, A., Merchán, M. E., Domínguez, M. 2002, MNRAS, 337, 1441

Merchán, M. E., Zandivarez, A. 2002, MNRAS, 335, 216

Miller, G. E., Scalo, J. M. 1979, ApJS, 263, 259

Moore, B., Governato, F., Quinn, T., Stadel, J., Lake, G. 1998, ApJ, 499L, 5

Navarro, J. F., Frenk, C. S., White, S. D. M. 1995, MNRAS, 275, 720

Navarro, J. F., Frenk, C. S., White, S. D. M. 1997, ApJ, 490, 493

Norberg, P., et al (2dFGRS Team), 2002, MNRAS, 336, 907

Press, W. H., Flannery, B. P., Teukolsky, S. S. and Vettrling, W. T., Numerical Recipes, Cambridge University Press, 1986

Salvador-Solé, E., Sanromà, M. 1989, ApJ, 337, 636

Strauss, M. A., et al, 2002, AJ, 124, 1810

Whitmore, B., Gilmore, D. 1991, ApJ, 367, 64

Whitmore, B., Gilmore, D. Jones C., 1993, ApJ, 407, 489

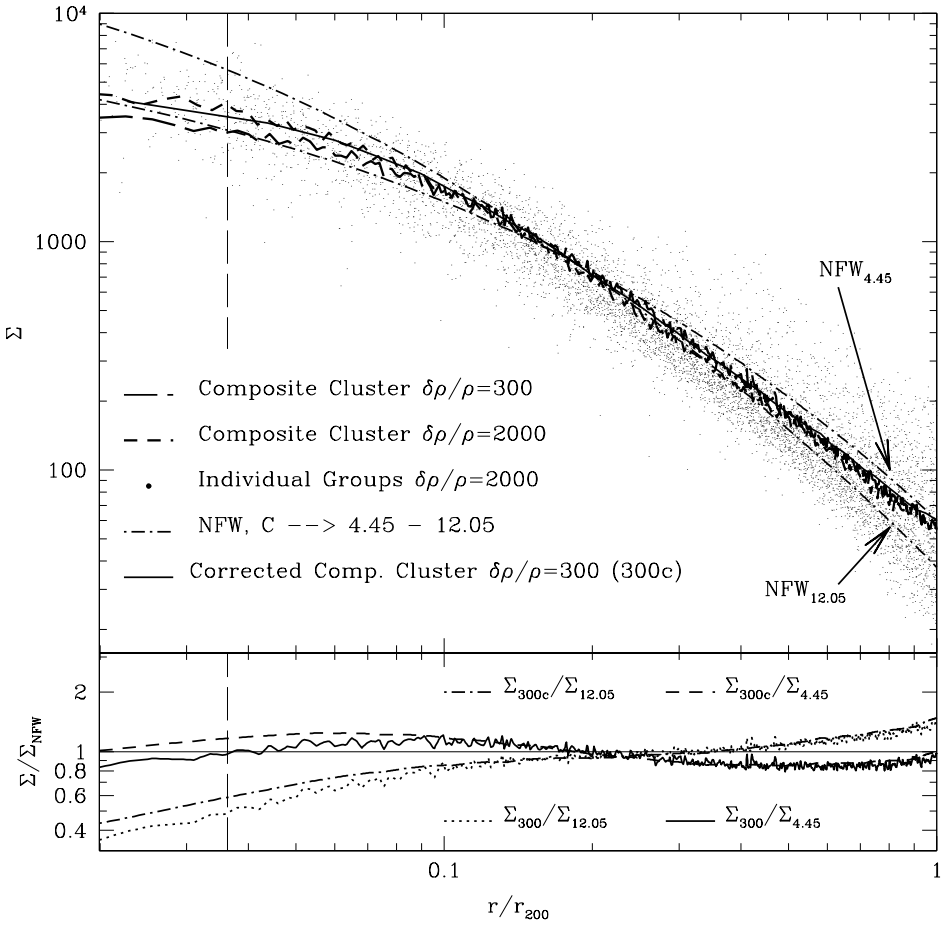

Fig. 1.— Upper panel: Projected density profiles as a function of the normalized group-centric distance. Long-dashed line is the measured projected density profile for the composite sample using groups identified with $\delta\rho/\bar{\rho} = 300$ while short-dashed line is the corresponding for groups obtained using $\delta\rho/\bar{\rho} = 2000$. The solid line is the measured projected density profile for groups identified with $\delta\rho/\bar{\rho} = 300$ after a correction made on the group center location. Single group projected density profiles for $\delta\rho/\bar{\rho} = 2000$ are shown as points. Projected NFW profiles are drawn with dot-dashed lines using c of 4.45 and 12.05. Lower panel: Ratios between measured profiles and NFW predictions as a function of r/r_{200}. The key of each curve is included in the figure. The subscripts represent the $\delta\rho/\bar{\rho}$ and the c parameter for the measured profiles and the NFW respectively.

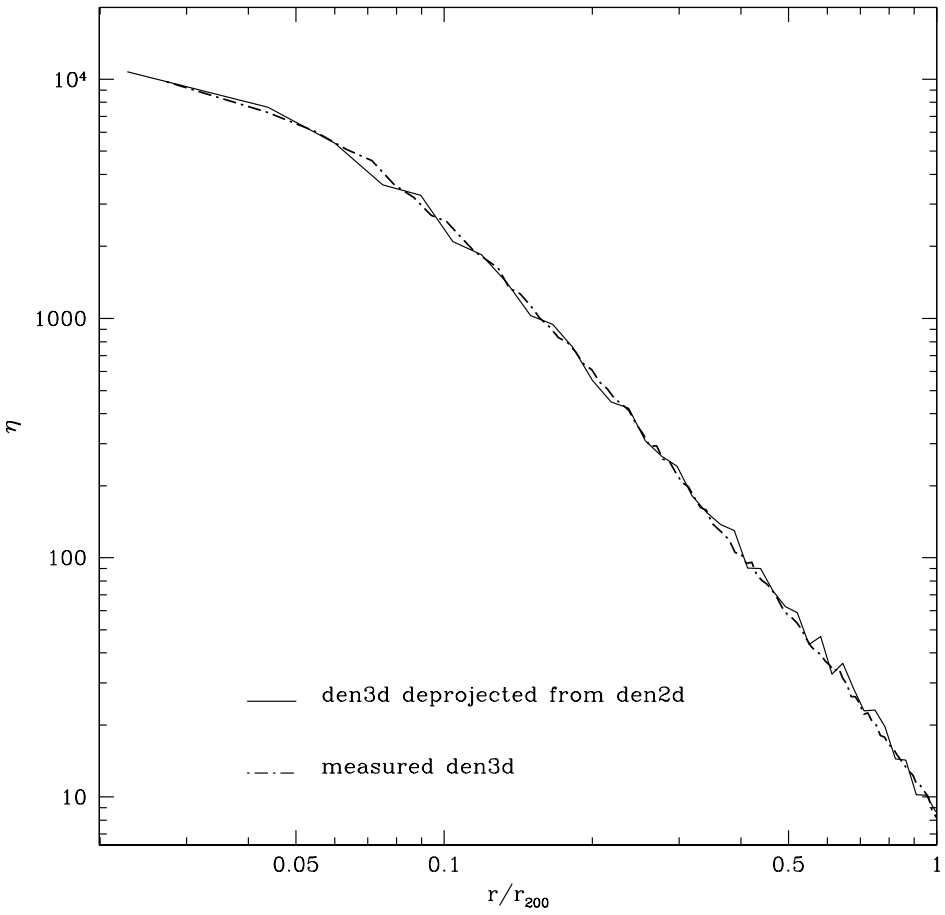

Fig. 2.— Deprojected density profiles for DM groups. The 3-D density profile calculated from the 2-D density profile using the deprojection method is shown as solid line. Dot-dashed line corresponds to 3-D density profile measured directly for the composite sample.

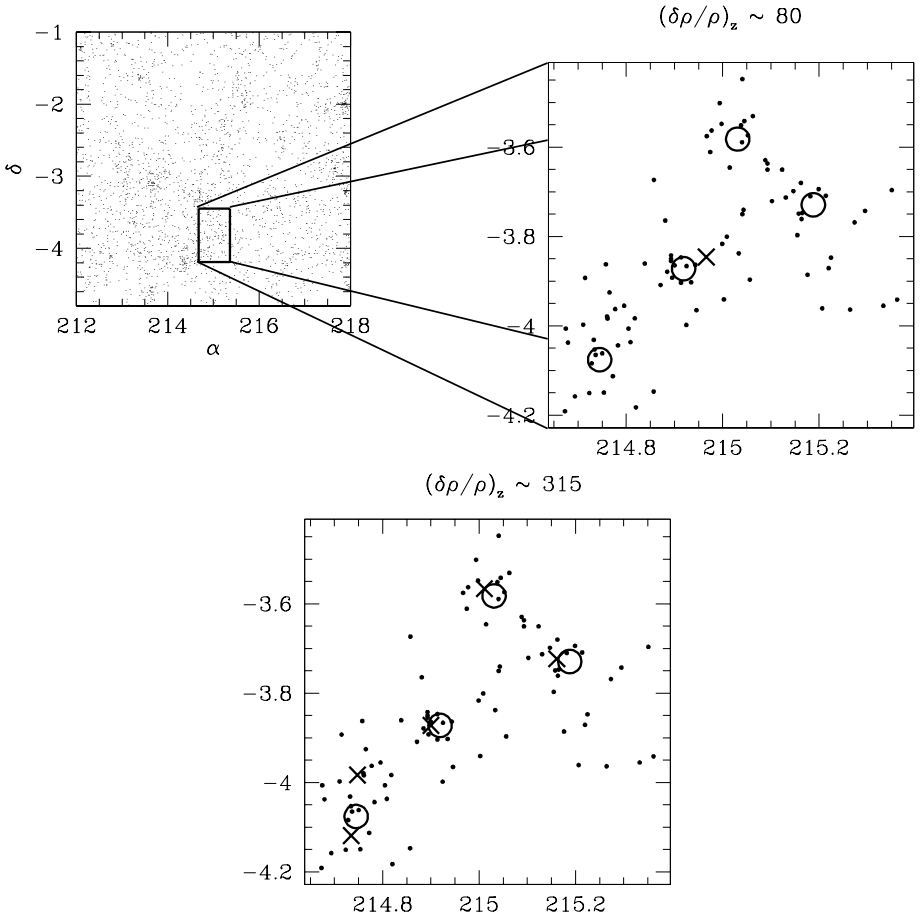

Fig. 3.— Comparison of groups identified in real and redshift space. Right upper panel shows, for a given patch on the sky, groups identified in real space with open circles while groups identified in redshift space are drawn with crosses. These identifications were performed using the same density contrast ($\delta\rho/\bar{\rho} \sim 80$). Dots are the galaxies belonging to the groups identified in redshift space. Lower panel shows a similar comparison as showed in the previous panel but now crosses denote the resulting sample of groups in redshift space after performing a second identification on the first sample of groups using $\delta\rho/\bar{\rho} \sim 315$.

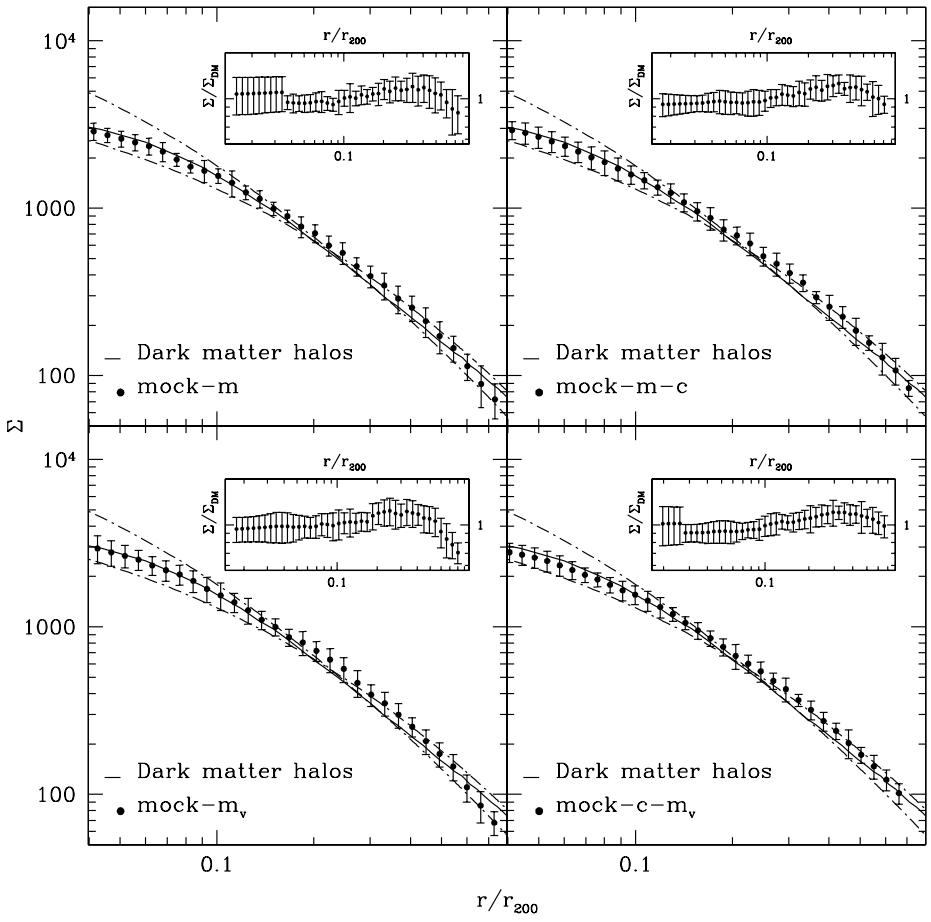

Fig. 4.— Projected density profiles measured for composite samples from mock catalogs. The left upper panel shows with points the averaged projected density profile measured for composite samples obtained from 10 mock-m catalogs (see the text). Right upper, left lower and right lower panels show the same profiles as left upper panel but measured for mock-m-c, mock-m_v and mock-c-m_v respectively. Error bars are computed measuring the dispersion for each set of mock catalogs. Solid line in each panel corresponds to the projected density profile computed using groups identified in the dark matter N-body simulations. Dot-dashed lines in each panels are projected NFW density profiles as plotted in Figure 1. The inset panels show the ratio between the averaged projected density profiles and the projected density profile obtained from the dark matter halos.

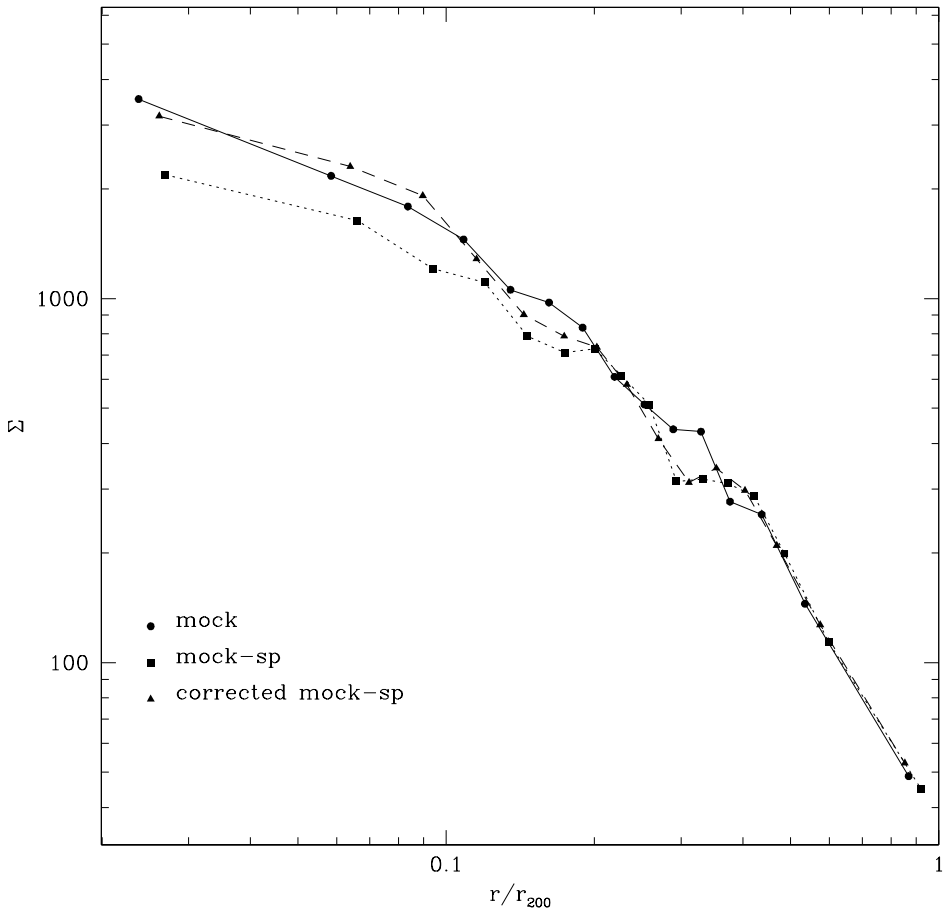

Fig. 5.— Projected density profiles measured from mock catalogs of the SDSS. Circles show the profile from a mock catalog which includes all galaxy pairs, squares are the profile of a mock catalog without 70 % of the pairs (mock-sp), while triangles are the corresponding profile to the mock-sp corrected by the missing close pairs.

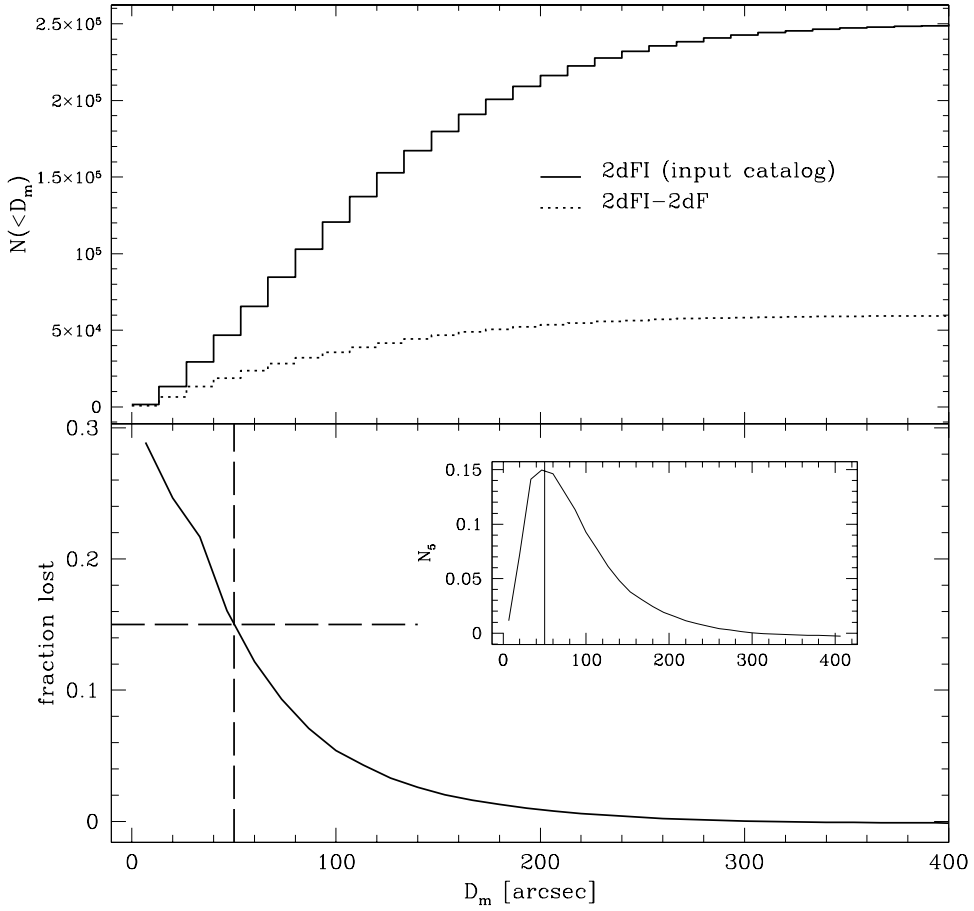

Fig. 6.— Upper panel: Cumulative galaxy distributions as a function of the angular distance to the nearest neighbor. Solid line represents the distribution for 2dFGRS input catalog (2dFI) while dotted line shows the distribution for 2dFI galaxies that are not included in the 2dFGRS. Lower panel: Cumulative fraction of lost galaxies in the 2dFGRS as a function of the minimal angular distance. Vertical dashed line determines the maximum angular distance $D^*_{m_{2dF}}$ adopted for the missing-pair correction in the 2dFGRS. Inset panel: Distribution of missed galaxies in groups as a function of D_m due to the missing-pair problem.

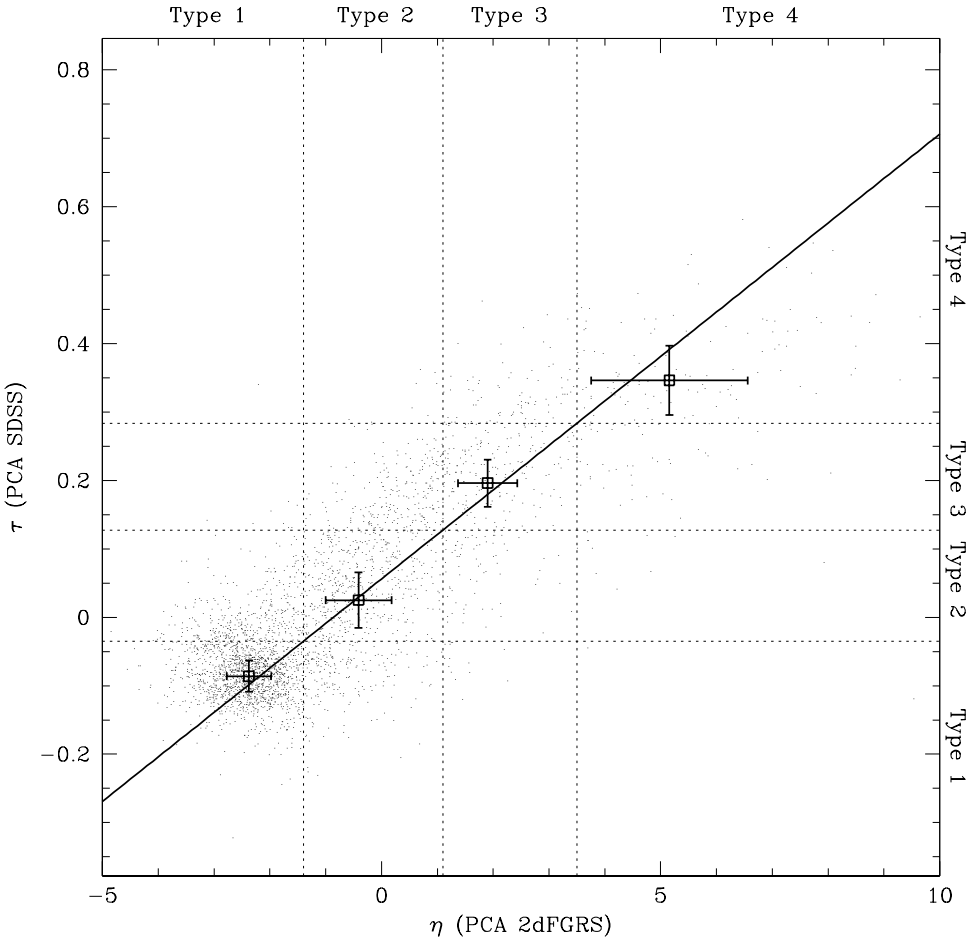

Fig. 7.— Correlation between the PCA spectral parameter η (2dFGRS) and τ (SDSS). The straight line is the linear fit to the data points. The open squares are the median η and τ values per spectral type, whereas the error bars are the semi-interquartile ranges.

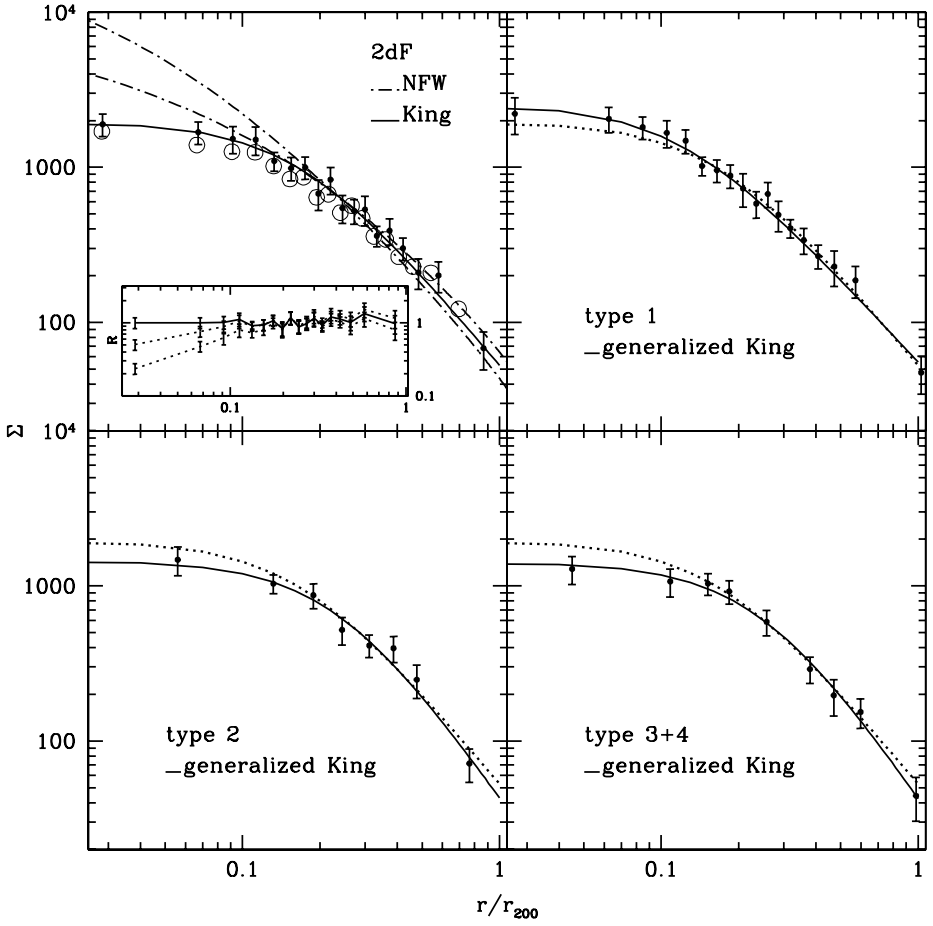

Fig. 8.— 2dF projected galaxy density profiles as a function of a normalized group-centric distance. Left upper panel shows the projected density profile (filled circles) measured for the whole composite sample. Open circles are the profile measured without introducing the missing-pair correction. In this panel, dot-dashed lines are the projected NFW profiles that expands the range of masses of physical relevance as the shown in Figure 1. Projected density profiles for spectral types 1, 2, 3 + 4 are shown in right upper, left lower and right lower panels respectively. The solid lines in each panel are King and generalized King fits with best-fitting parameters quoted in Table 2. We also plot with dotted line in the panels per spectral type the profile fitted for the complete composite sample. The inset box in the left upper panel shows the ratio between the observational projected density profile and the best-fit King (solid line) and the two reference NFW (dotted lines) profiles.

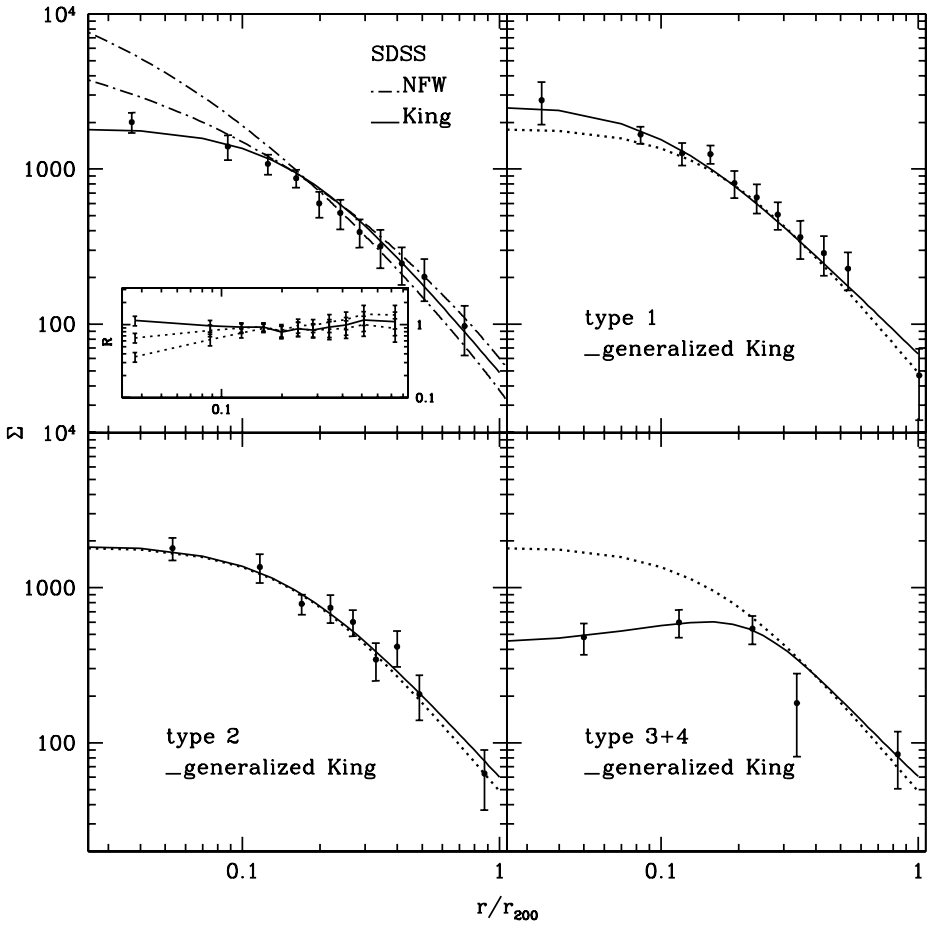

Fig. 9.— Same as Figure 8 but measured for the SDSS composite sample.

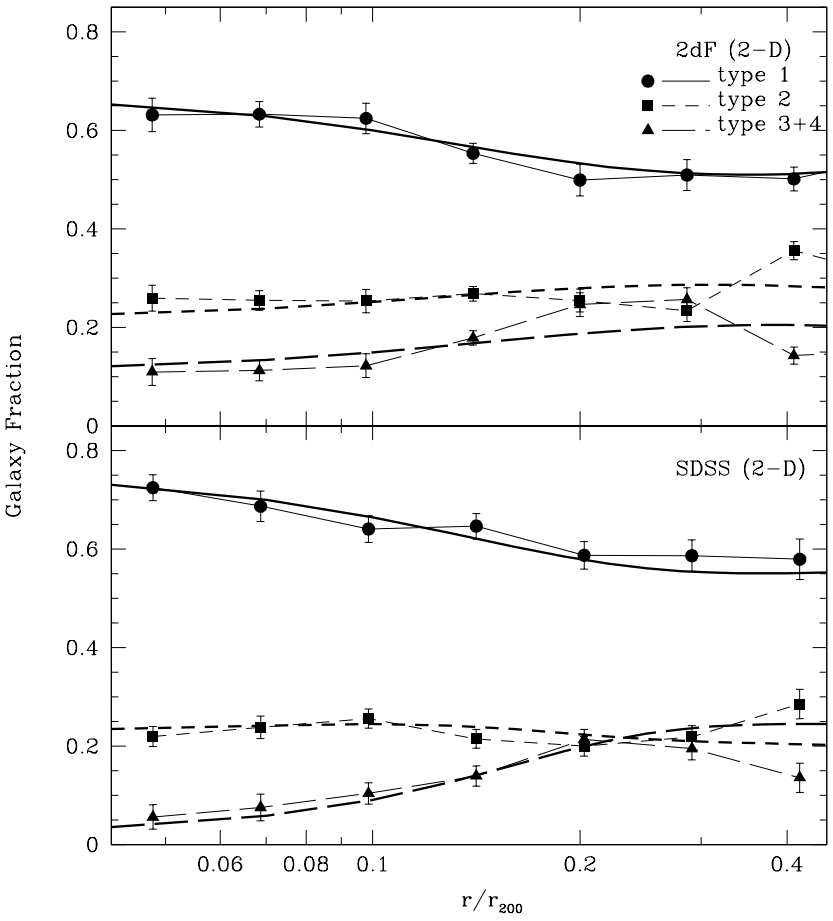

Fig. 10.— 2-D fractions of galaxies of different spectral types as a function of the normalized group-centric distance for the 2dF (upper panel) and the SDSS (lower panel). The key for the different spectral types is included in the figure. Error bars are computed from error propagation. Thick lines correspond to the galaxy fractions computed from the generalized King profiles fitted to the projected density profiles.

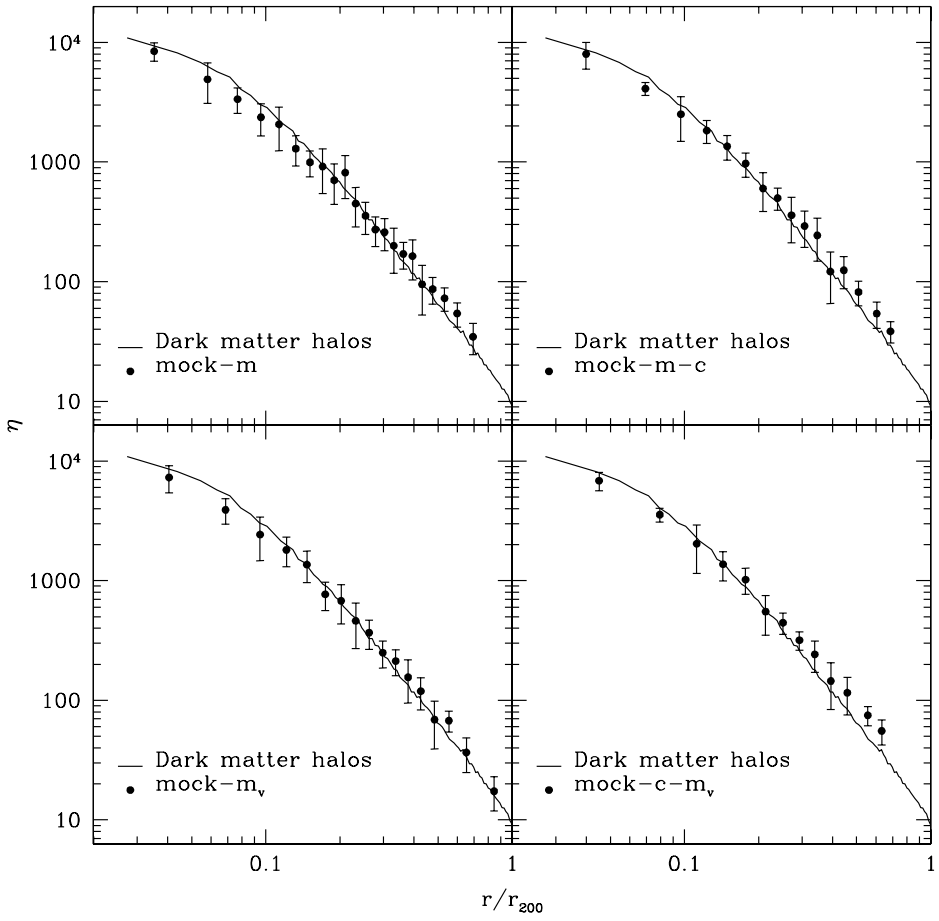

Fig. 11.— Average deprojected galaxy density profiles obtained from the projected galaxy density profiles of mock catalogs showed in Figure 4. The points in the left upper panel show the average value of the deprojection of ten 2-D profiles obtained from mock-m catalogs. Error bars are the associated $1-\sigma$ dispersion. Right upper, left lower and right lower panels show the same profiles as in the left upper panel but obtained from mock-m-c, mock-m_v and mock-c-m_v respectively. Solid line in each panel corresponds to the deprojected density profile obtained from the projected density profile computed for groups identified in the dark matter N-body simulations.

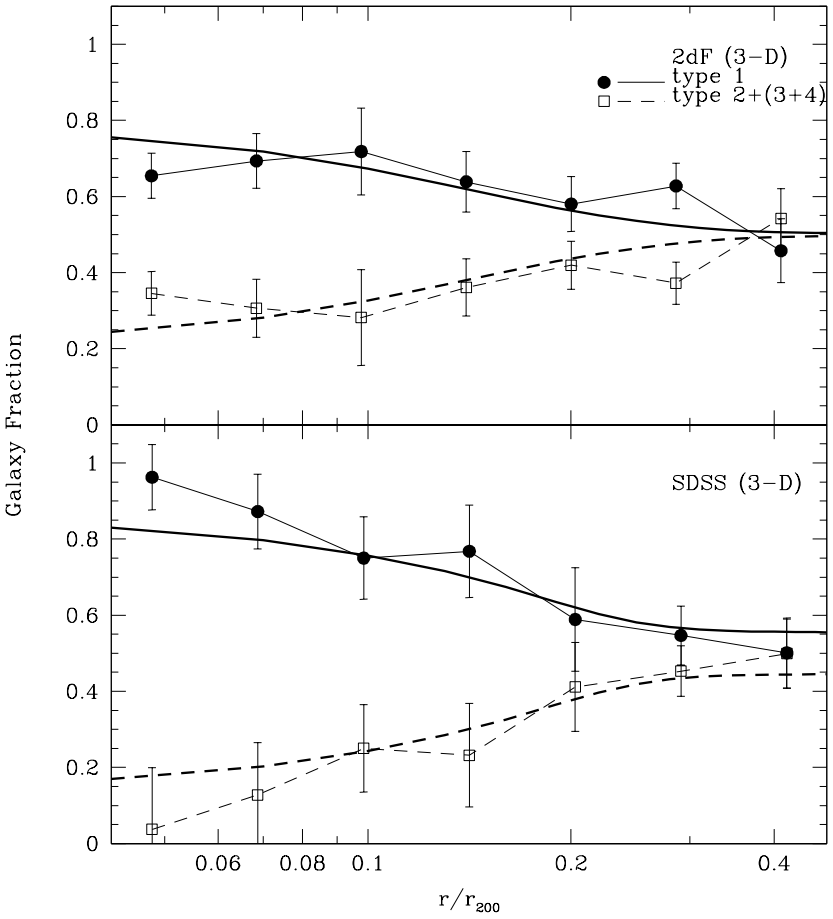

Fig. 12.— 3-D fraction of galaxies per spectral type as a function of the normalized group-centric distance for the 2dF (Upper panel) and for the SDSS (Lower panel). The key for the different spectral types is included in the figure. Error bars are computed from error propagation. Thick lines correspond to the galaxy fractions computed from the generalized King profiles (see text).

Table 1. Median group properties and distribution widths for the group samples.

	2dFGRS				SDSS			
	z	σ $[km\ s^{-1}]$	M_{vir} $[M_\odot\ h^{-1}]$	R_{vir} $[Mpc\ h^{-1}]$	z	σ $[km\ s^{-1}]$	M_{vir} $[M_\odot\ h^{-1}]$	R_{vir} $[Mpc\ h^{-1}]$
median	0.09	442	8.7×10^{13}	0.9	0.08	427	9.3×10^{13}	0.9
width	0.03	133	1.2×10^{14}	0.3	0.03	159	1.6×10^{14}	0.4

Table 2: Best-fitting parameters for the projected galaxy density profiles. Parameters without error were fixed in the fitting process. The last three columns show the degrees of freedom, the chi-square value of the fits and the Q probability.

Catalog	sample	Ngal	c	β	x_0	ν	χ^2	Q
2dF (132)	total	2277	6.0 ± 0.2	1.0	0.0	17	13.73	0.68
	type 1	1710	8.3 ± 0.3	0.90 ± 0.05	0.0	16	9.55	0.89
	type 2	339	4.2 ± 0.5	1.2 ± 0.1	0.0	6	7.13	0.31
	type 3+4	228	4.0 ± 0.4	1.2 ± 0.1	0.0	7	4.46	0.72
SDSS (86)	total	2031	6.1 ± 0.3	1.0	0.0	10	10.50	0.40
	type 1	1543	9.8 ± 0.2	0.8 ± 0.1	0.0	9	10.54	0.31
	type 2	364	6.6 ± 0.5	0.9 ± 0.1	0.0	7	8.54	0.29
	type 3+4	124	5.8 ± 0.8	0.7 ± 0.2	0.15 ± 0.06	2	6.02	0.05